Synthesis and characterization of nickel nanoparticles anchored on chemically functionalized carbon nanotubes

M. STANCU[a], G. RUXANDA[a], N. STANICA[b], A. DINESCU[c], D. CIUPARU[a]
[a] *Petroleum-Gas University of Ploiesti, 39 Bucuresti Blv., 100680, Ploiesti, Romania*
[b] *Institute of Physical Chemistry "Ilie Murgulescu", Bucharest, Romania*
[c]*National Institute for Research and Development in Microtechnologies, Bucharest, Romania*

A simple method for anchoring nickel particles on chemically functionalized carbon nanotubes using nickel(II) nitrate hexahydrate is described. The functionalization is accomplished in three main steps and leads to carbon nanotubes with nickel nanoparticles attached on the walls. The structural properties of the resulting material were characterized by X-Ray diffraction (XRD), Fourier transform infrared spectroscopy (FTIR), Raman spectroscopy, Scanning electron microscopy (SEM) and Transmission electron microscopy (TEM), while their magnetic properties were measured at room temperature using a vibrating - sample magnetometer. The results obtained are discussed.

(Received December 14, 2012; accepted February 20, 2013)

Keywords: Functionalized carbon nanotubes, Chemical treatment, Vibrating sample magnetometer, Magnetic hysteresis, System superparamagnetic

1. Introduction

Carbon nanotubes are large macromolecules unique for their size, shape, and remarkable physical properties, and were discovered in 1991 by S. Iijima [1]. The intrinsic properties of carbon nanotubes can be modified by functionalization of their surface. After functionalization the resulting material can be used to develop applications in various areas [2]. Any functionalization of carbon nanotubes determines changes in properties such as solubility, conductivity, magnetism, etc., thus making nanotubes applicable for different purposes. Among other functional species, metal nanoparticles have attracted much attention. Carbon nanotubes functionalized with metallic nanoparticles can be used as electronic devices, catalysts, magnetic storage devices and sensors [3–6].

The main purpose in this contribution was to investigate the magnetic properties of the CNT functionalized with nickel nanoparticles. The magnetic properties of the resulting material consisting of nickel nanoparticles attached to carbon nanotubes have been characterized by Vibrating - sample magnetometer (VSM). The structure and morphology of the nickel nanoparticles attached on the sidewalls of the carbon nanotubes were also characterized and the results are discussed.

2. Experimental

The carbon nanotubes used in this work are produced by the AC arc discharge method described elsewhere [7], and subsequently purified by hydrochloric acid followed by air oxidation, as previously reported [8].

The synthesis procedure of nickel nanoparticles attached to carbon nanotubes is schematically presented in Fig. 1, while Fig. 2 shows the subsequent thermal treatment. In principle, this procedure consists of a series of steps. The pristine carbon nanotubes are firstly refluxed in nitric acid (36%) for 3 h at 105°C. After filtration, washing and drying at 70°C for 24 h, the resulting product was coded as D_Ar_step1. Nickel(II) nitrate hexahydrate ($Ni(NO_3)_2 \cdot 6H_2O$) (0.70 g, 0.24 mmol) was dissolved in 20 ml of ethanol and then the sample D_Ar_step1 was dispersed in the resulting solution for 1h using an ultrasonic probe. The material was then dried at 70°C for 24 h to avoid aggregation and denominated as D_Ar_Ni_step2. Finally, the sample D_Ar_Ni_step2 was placed into a quartz reactor and a thermocouple was inserted directly into the sample bed. A hydrogen flow was passed over the carbon nanotubes from the beginning of the thermal treatment. The nickel compounds on the walls of the nanotubes are decomposed and reduced to form pure nickel nanoparticles. At the end of the thermal treatment depicted in Fig. 2 the hydrogen flow was ceased and the quartz reactor was cooled down slowly to the room temperature under Ar flow. The resulting material in the quartz reactor was coded as D_Ar_Ni_step3. To demonstrate that nickel nanoparticles were formed and actually attached on the carbon nanotubes sidewalls, we used different characterization techniques such as: X-Ray diffraction (XRD), Fourier transform infrared spectroscopy (FTIR), Raman spectroscopy, Scanning electron microscopy (SEM), and Transmission electron microscopy (TEM). We have also used a Vibrating - sample magnetometer (VSM) to characterize the magnetic properties of the resulting material.

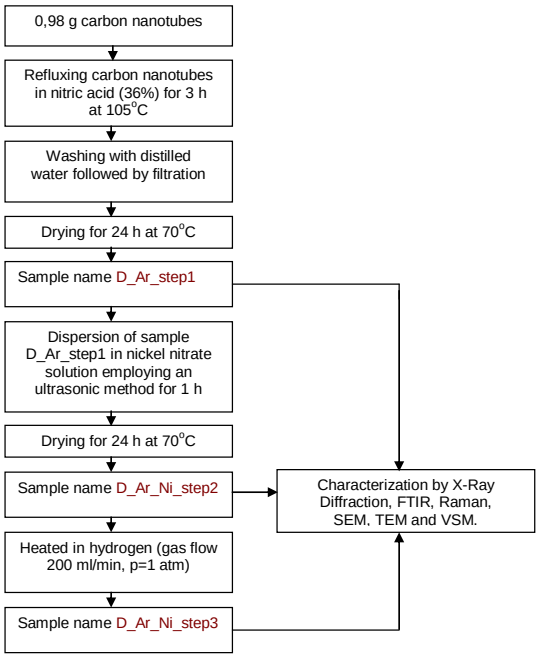

Fig. 1. Schematic of the procedure of synthesis of nickel nanoparticles attached to carbon nanotubes.

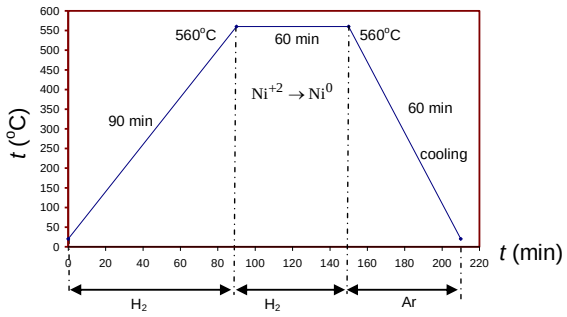

Fig. 2. Thermal treatment.

3. Results and discussion

The structural characteristics of the materials have been analyzed by powder X-ray diffraction measurements carried out on a D8ADVANCE Nova diffractometer using the characteristic radiation Kα of copper, at a voltage of 40 kV and 40 mA intensity. The sweeping of angles was carried out between 5 and 80 degrees, with 0.01 degrees incremental steps at 1 s per step for all measurements. XRD data was also used to assess the crystallite size of the metallic particles by the Debye-Scherrer formula.

The X-ray diffractograms of the D_Ar_step1, D_Ar_Ni_step2 and D_Ar_Ni_step3 samples are shown in Fig. 3. The diffraction peak at $2\theta=26^{o}$ observed in all diffractograms for the carbon nanotubes are attributed to the hexagonal graphite structures corresponding to the (002) plane (black arrow) [9]. After the second and third steps of the functionalization procedure other diffraction peaks can be observed in the corresponding diffractograms. Blue arrows mark the appearance of new peaks in the X-ray diffractogram of the D_Ar_Ni_step2 sample in the angular domains from 10 to 23^{o} and from 30 to 40^{o}, respectively, and these correspond to the nickel(II) nitrate [10]. These peaks are not observed in the diffractogram of the D_Ar_Ni_step3 sample because during the third step of the functionalization procedure nickel nanoparticles are generated by the reduction of nickel(II) nitrate with hydrogen. Peaks at 44.6°, 51.9° and 76.5° (red arrows) are observed in the diffractogram of the D_Ar_Ni_step3 sample. These peaks are assigned to (111), (200) and (220) diffraction planes of nickel nanoparticles according to previously reported studies [11]. The average crystallite size of the nickel nanoparticles, as determined with the Debye-Scherrer formula, varies from 15 to 50 nm, in good agreement with the size distribution observed in TEM.

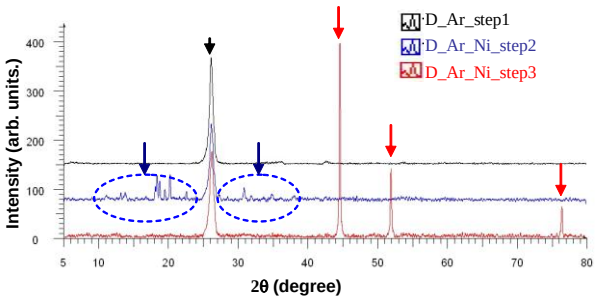

Fig. 3. X-ray difractograms of D_Ar_step1, D_Ar_Ni_step2, D_Ar_Ni_step3 samples.

To study the changes occurring in the carbon nanotubes passing through the three stages of the functionalization procedure, Fourier-transform infrared (FTIR) spectra were recorded with an attenuated total reflection (ATR) device on a Varian 3100 Escalibur FT-IR instrument.

Fig. 4 shows the comparative FT-IR spectra of the D_Ar_step1, D_Ar_Ni_step2 and D_Ar_Ni_step3 samples. The FT-IR spectra were collected in the wavenumber range from 1400 to 1900 cm^{-1}.

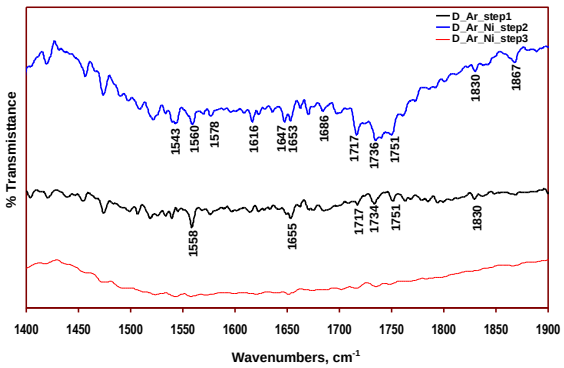

Fig. 4. FTIR spectra of D_Ar_step1, D_Ar_Ni_step2, D_Ar_Ni_step3 samples.

A C=O stretching absorption band can be observed in the region 1540-1870 cm^{-1} of the FT-IR spectra of the D_Ar_step1 and D_Ar_Ni_step2 samples. Changes in the

environment of the carbonyl group can either lower or raise the absorption frequency in this region [12].

The FT-IR spectrum recorded for sample D_Ar_Ni_step3 does not show the presence of C=O stretching modes for carbonyl groups, meaning that, after heating in hydrogen, the oxygen was removed from the functional groups, in agreement with previous reports [3].

Surface carbonyl or carboxyl functional groups make the carbon nanotubes amenable to anchor precursors of highly dispersed metal nanoparticles, as already reported by other authors [13, 14], thus, the carbon nonotubes resulting after the acid treatment are ready to anchor chemical moieties containing metallic ions that can be converted into dispersed metallic clusters.

Raman spectroscopy was also used to characterize the structure of our samples. Raman spectra were recorded using a single excitation wavelength at 532 nm on a NRS-3000 Raman equipment from Jasco.

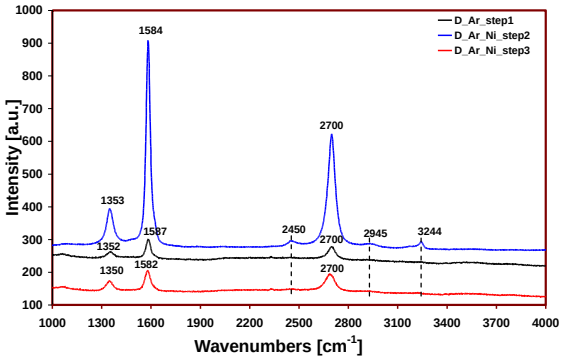

Fig. 5. Raman spectra of D_Ar_step1, D_Ar_Ni_step2, D_Ar_Ni_step3 samples.

The first and second-order Raman spectra of our samples are displayed in Fig. 5. The first order Raman spectra show a strong peak around 1580 cm^{-1} associated with hybridized sp^2 carbon domains (G-band) [15, 16], which is the high-frequency E_{2g} first-order Raman mode. A peak at approximately 1350 cm^{-1} is also visible. This peak is generally attributed to defective or disordered structures and is termed D (disordered) band [17-20]. The intensity ratio between D and G bands (I_D/I_G ratio) is widely accepted as a good indicator for the quality of bulk samples [21]. The intensity ratio I_D/I_G was found 0.954 for sample D_Ar_step1, 0.962 for sample D_Ar_Ni_step3 and only 0.433 for sample D_Ar_Ni_step2. All these I_D/I_G values are lower than 1. Compared to the other two samples, D_Ar_Ni_step2 has a much smaller intensity ratio indicating that the defect level in the carbon structure is low, which suggests reasonable crystalline quality [22, 23].

The G'-band is observed near 2700 cm^{-1} in the second order Raman spectra for all samples. It is worth noting that the spectrum of sample D_Ar_Ni_step2 shows more intense peaks for other main lines of the second order Raman spectra compared with the other two samples. We observed strong peaks at 2450 cm^{-1}, 2945 cm^{-1} and 3244 cm^{-1}, with the later two being attributed to (D+G) and (2D') modes, respectively [17]. The peak at 2450 cm^{-1} most likely belongs to the band as D (1350 cm^{-1}) + D" (1090 cm^{-1}) [24-27].

The morphology of the carbon nanotubes after each stage of functionalization was observed by scanning electron microscopy using a Nova NanoSEM 630 equipment, and by transmission electron microscopy performed on a TEM-EM-410 microscope from PHILIPS.

The outer-surface morphology of carbon nanotubes can be observed in the micrographs in Fig. 6. The SEM images of samples D_Ar_step1 and D_Ar_Ni_step2 do not show any modifications of the outer-surface of the carbon nanotubes, as seen in Fig. 6 (a) and (b).

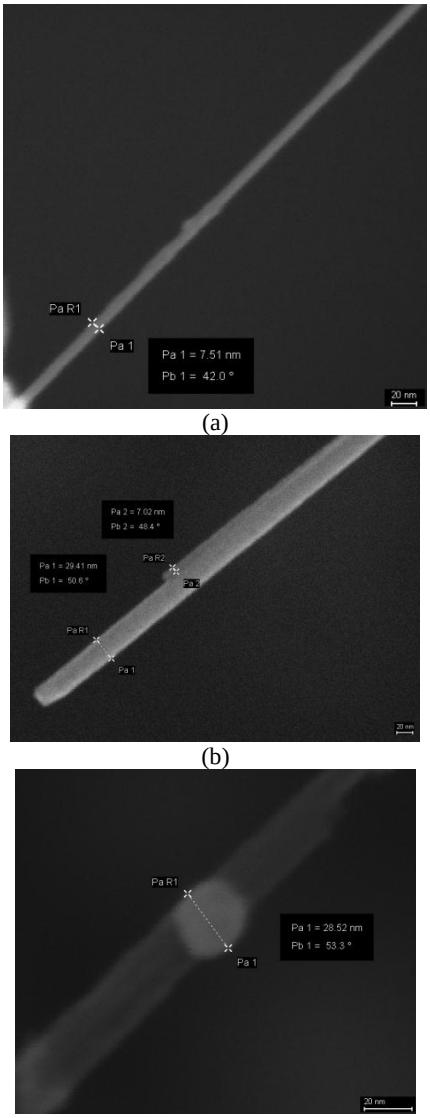

Fig. 6. SEM images of samples: (a). D_Ar_step1; (b). D_Ar_Ni_step2; (c). D_Ar_Ni_step3.

Fig. 6 (a) shows a carbon nanotube with an outer diameter of ~7.51 nm, while in Fig. 6 (b) two adjacent carbon nanotubes with outer diameters of ~7 nm and ~29nm, respectively, can be observed. Fig. 6 (c) shows the SEM image of a carbon nanotube with a nickel nanoparticle attached on its wall. This metal nanoparticle

has an outer diameter of approximately 29 nm.

Anchoring of nickel nanoparticles onto the surface of carbon nanotubes was also confirmed by Transmission electron microscopy (TEM). TEM images show that the morphologies of the three samples are different. Fig. 7 shows TEM images of D_Ar_step1, D_Ar_Ni_step2 and D_Ar_Ni_step3 samples at different magnifications.

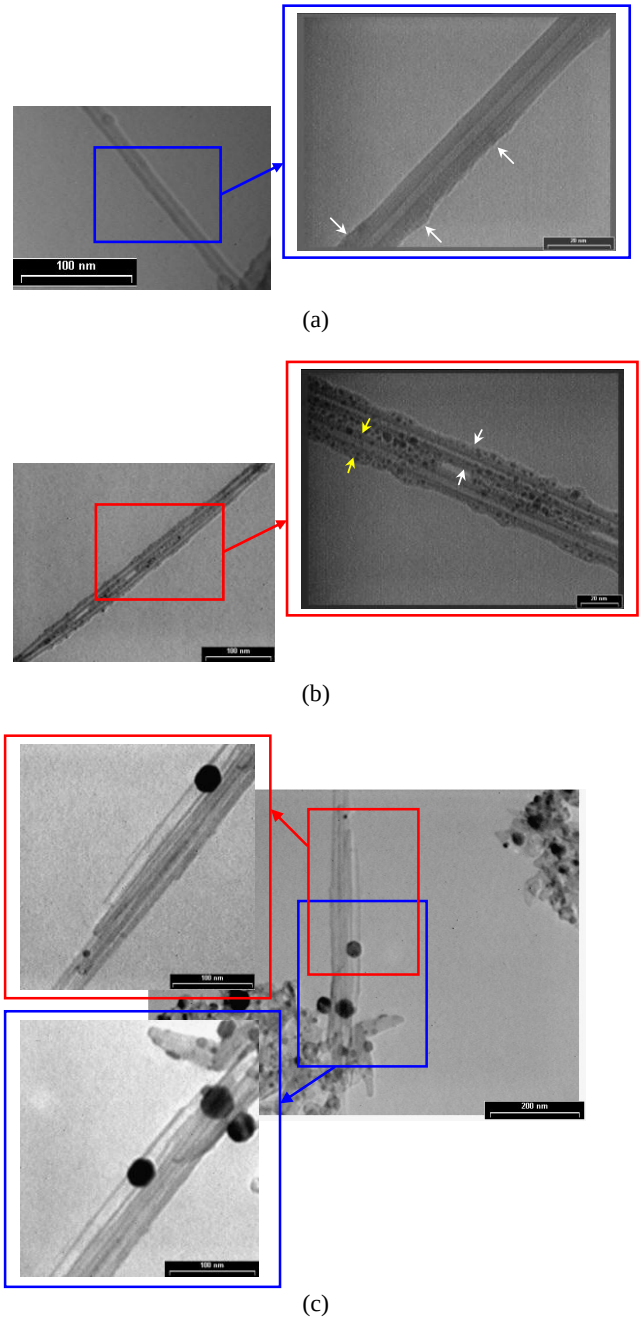

Fig. 7. TEM images of samples:
(a). D_Ar_step1; (b). D_Ar_Ni_step2; (c). D_Ar_Ni_step 3.

The rough surface indicated by the white arrows in Fig. 7(a) suggests the carbon nanotube has functional groups attached on the outer-surface resulting after the nitric acid treatment. Fig. 7(b), on the other hand, shows two carbon nanotubes that have a thick layer of material deposited on their external surface as indicated by the white and yellow arrows. The outer deposit resulting after the second step of functionalization procedure most likely consists of a layer of nickel nitrate anchored on surface carbonyl and/or carboxyl groups. However, the clear evidence for the anchoring of nickel nanoparticles on the surface of carbon nanotubes is provided by the TEM images shown in Fig. 7(c). The morphology of both nickel nanoparticles and carbon nanotubes are clearly observed. Nickel nanoparticles of a rather wide distribution of sizes are attached on the walls of carbon nanotubes. The size of the nickel nanoparticles lies in the range of 15 to 50 nm.

The magnetic properties of the synthesized samples were measured at room temperature using a vibrating sample magnetometer (VSM; Lake Shore) at a maximum applied field of 10 kOe. Significant modifications in the magnetic properties of our samples were observed during these measurements. The magnetic behavior of samples D_Ar_step1, D_Ar_Ni_step2 and D_Ar_Ar_step3 are shown in Figs. 8, 9 and 10, respectively. The diamagnetic behavior of the D_Ar_step1 sample can be observed in Fig. 8. This behavior can be attributed to the pure carbon nanotubes [28, 29]. Diamagnetism is due to induced currents opposing an applied field resulting in a small negative magnetic susceptibility, χ. For sample D_Ar_step1, the value found for the magnetic susceptibility was: $\chi = (-6.80 \pm 0.12) \times 10^{-6}$ cm^3 / g .

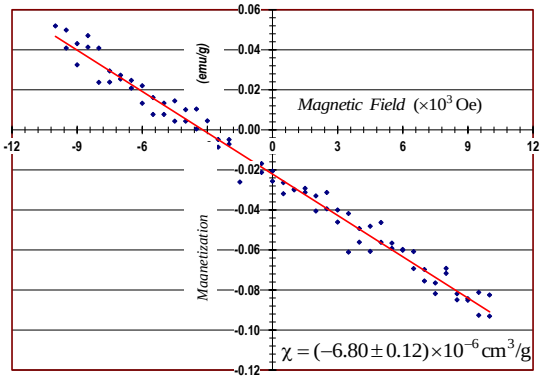

Fig. 8. Diamagnetic behavior of D_Ar_step1 sample.

Fig. 9 shows the paramagnetic behavior of the D_Ni_step2. The different behavior of D_Ni_step2 sample leads us to conclude that, after the second stage of functionalization, the sample contains Ni^{2+} ions. Sample D_Ar_Ni_step2 has a small positive value of the susceptibility to the applied magnetic field, $\chi = (1.26 \pm 0.16) \times 10^{-6}$ cm^3 / g . The paramagnetic behavior shows that sample D_Ar_Ni_step2 is slightly attracted by the magnetic field and it does not retain the magnetic properties when the external field is removed. The paramagnetic properties are due to the presence of unpaired electrons, and from the realignment of the electron paths caused by the application of an external magnetic field.

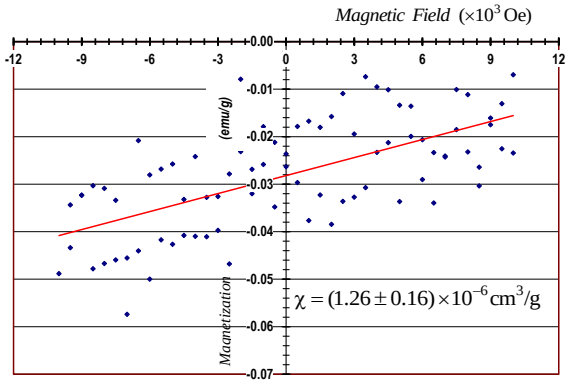

Fig. 9. Paramagnetic behavior of D_Ar_Ni_step2 sample.

Compared to the other two, sample D_Ar_Ar_step3 shows hysteretic behavior, as observed in Fig. 10. The magnetic field measured as a function of magnetization at room temperature is recorded at a field strength varying from +10 kOe to -10 kOe.

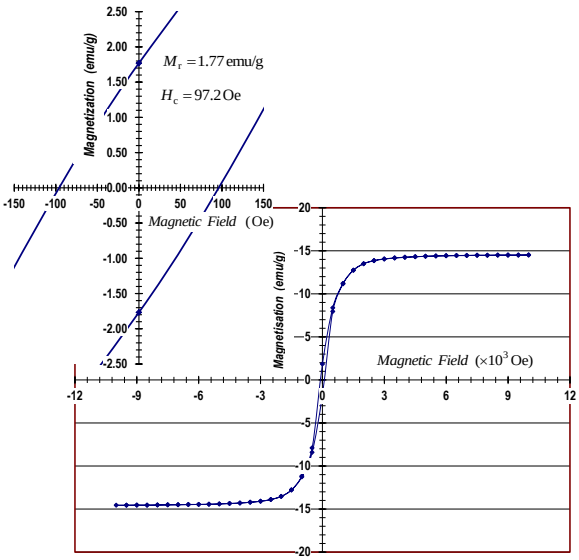

Fig. 10. Magnetic hysteresis curve measured at a room temperature for the D_Ar_Ni_step3 sample

The analytical techniques employed to characterize the particle size distribution showed particle diameters varying from 15 to 50 nm. Particles of smaller size, centered near 15 nm, are often considered magnetic single domains showing a single giant magnetic moment formed by an exchange interaction between all individual spins [30-32], while those of larger sizes have few magnetic domains. Because the larger particles have only a small number of magnetic domains, they have a lower characteristic magnetic moment compared to the single magnetic domain particles.

The shape of the hysteresis loop is determined partly by the domain state. Loops for single domain materials are typically wider than loops for magnetic multi domain materials [33]. This is just a reflection of the higher coercivity and remanence in single domain materials [33]. From the hysteresis loop obtained, the ratio between the remanent and the saturation magnetizations (M_r/M_s), and the coercivity (H_c) were measured and found 0.121 and 97.2 Oe, respectively. These results are in good agreement with those reported for Ni particle aggregates or magnetic clusters with grain sizes near 20 nm showing M_r/M_s=0.170 and coercivity of 86.5 Oe [34], while for Ni powders of 80 nm, values of 0.182 and 68.11 Oe were found for M_r/M_s and coercivity, respectively [35]. For low magnetic fields below 2400 Oe, magnetization increases rapidly towards the saturation level, as observed in [34], and, also similarly, the area of the hysteresis loop is very low.

All these observations indicate the hybrid material obtained by anchoring Ni nanoparticles 15 to 50 nm in size on carbon nanotubes shows superparamagnetic behavior rather than ferromagnetic behavior as one might expect in such a system. Thus, the product resulting from the third synthetic stage, shows superparamagnetic behavior at temperatures of 300K most likely resulting from the combination of the ferromagnetic behavior of the Ni nanoparticles and the diamagnetic properties of their carbon nanotubes support. Such behavior has been previously reported for Ni nanoparticles isolated in diamagnetic matrices [30], [32], [36], [37].

3. Conclusions

A simple method is described to anchoring nickel nanoparticles on the walls of carbon nanotubes. The first step of this method, consisting of the oxidation of the outer-surface of carbon nanotubes using nitric acid, makes possible the formation of carbonyl and carboxyl functional groups on the walls of carbon nanotubes.

The second and the third synthetic steps allowed anchoring the nickel precursor and the formation of metallic nickel nanoparticles anchored on the nanotube walls. The nickel precursors deposited on carbon nanotubes resulting after the second step of the functionalization procedure were reduced during the thermal treatment in hydrogen and produced nickel nanoparticles ranging from 15 to 50 nm, as confirmed by XRD, SEM and TEM analysis.

The hybrid nanostructured material obtained by our method raises special interest because, at 300K, shows superparamagentic properties. Such material can be used in a wide range of applications, such as catalysis, chemical/biological sensing, optoelectronics [38-40], nanoelectrode ensembles, sensors, and biocatalysis [41-44].

Acknowledgements

The authors acknowledge the financial support from the European Social Fund through the POSDRU/89/1.5/S/54785 project: "Postdoctoral Program for Advanced Research in the field of nanomaterials".

The VSM instrument has been purchased with financial support from the European Regional

Development Fund through program POSCCE O 2.2.1 project / INFRANANOCHEM - Nr. 19/01.03.2009.

References

[1] S. Iijima, Nature **354**, 56 (1991).
[2] S. Banerjee, T. H. Benny, S. S. Wong., [J]. Advanced Materials, **17**, 17 (2005).
[3] A. Leela Mohana Reddy, S. Ramaprabhu, Nanoscale Res Lett, **3**, 76 (2008).
[4] G. Che, B. B. Lakshmi, C. R. Martin, E. R. Fisher, Langmuir **15**, 750 (1999).
[5] J. Sloan, J. Cook, M. L. H. Green, J. L. Hutchison, R. Tenne, J. Mater. Chem. **7**, 1089 (1997)
[6] R. Kozhuharova, M. Ritschel, D. Elefant, A. Graff, I. Monch, T. Muhl, C. M. Schneider, A. Leonhardt, J. Magn. Magn. Mater. **290**, 250 (2005).
[7] G. Ruxanda et al., J. Optoelectron. Adv. Mater. **10**(8), 2047 (2008).
[8] M. Stancu, G. Ruxanda, D. Ciuparu, A. Dinescu, Optoelectron. Adv. Mater.-Rapid Commun., **5**(8), 846 (2011).
[9] Jipeng Cheng, Xiaobin Zhang, Ying Ye, Journal of Solid State Chemistry, **179**, 91 (2006).
[10] Yi Du, Amber L. Thompson, Nicola Russell, Dermot O'Hare, Dalton Trans., **39**, 3384 (2010).
[11] Burçak Ebin, Sebahattin Gurmen, KONA Powder and Particle Journal, **29**, 134 (2011).
[12] Robert M. Silverstein, Francis X. Webster, David J. Kiemle, Spectrometric identification of organic compounds, seventh edition, (John Wiley & Sons, INC., 2005).
[13] Hongjin Jiang, Lingbo Zhu, Kyoung-sik Moon, C. P. Wong, Carbon, **45**, 655 (2007).
[14] R. V. Hull, L. Li, Y. C. Xing, C. C. Chusuei., Chem Mater, **18**, 1780 (2006).
[15] R. Engel-Herbert, H. Pforte, T. Hesjedal, Materials Letters, **61**, 2589 (2007).
[16] R. Saito, G. Dresselhaus, M. S. Dresselhaus, Imperial College Press, London, (1998).
[17] E. F. Antunes, A. O. Lobo, E. J. Corat, V. J. Trava-Airoldi, A. A. Martin, C. Verissimo, Carbon, **44**, 2202 (2006).
[18] Z. Wang, X. Huang, R. Xue, L. Chen, J Appl Phys; **84**, 227 (1998).
[19] T. Beltn, F. Epron, Mat Sci. Eng. B, **119**, 105 (2005).
[20] R. J. Nemanich, S. A. Solin., Phys Rev B, **20** 392 (1979).
[21] Rahul Rao, et.al., Carbon, **49**, 1318 (2011).
[22] V. Shanov, Yeo-Heung Yun, M. J. Schulz, Journal of the University of Chemical Technology and Metallurgy, **41**, 4, 377 (2006).
[23] C. Singh, M. Shaffer, K. Kazoil, I. Kinloch, A. Wndle, Chemical Physics Letters, **372**, 860 (2003).
[24] T. Shimada et al. Carbon, **43**, 1049 (2005).
[25] P. H. Tan, Y. M. Deng, Q. Zhao, Phys Rev B, **58**(9), 5435 (1998).
[26] P. H. Tan, C. Y. Hu, J. Dong, W. C. Shen, B. F. Zhang, Phys Rev B, **64**(21), 214301-1–12, (2001).
[27] P. H. Tan, L. An, L. Q. Liu, Z. X. Guo, R Czerw, D. L. Carroll, et al., Phys Rev B, **66**(24), 245410-1–8, (2002).
[28] M. Stancu, G. Ruxanda, N. Stanica, A. Dinescu, L. Nistor, D. Ciuparu, Optoelectron. Adv. Mater. – Rapid Commun., **6**(7-8), 723 (2012).
[29] Kamil Lipert, et al., Journal of Applied Physics, 105, 063906 (2009).
[30] Sergey P. Gubin, Magnetic Nanoparticles, (Wiley-VCH, Verlag GmbH&Co.KGaA, ISBN: 978-3-527-40790-3, 2009).
[31] L. Dormann, D. Fiorani, E. Tronc, Adv. Chem. Phys., **98**, 283, (1997).
[32] D. Kumar, S. J. Pennycook, A. Lupini, G. Duscher, A. Tiwari, J. Narayan, Appl. Phys. Lett., **81**(22), 25 (2002).
[33] B. D. Cullity, C. D. Graham. Introduction to Magnetic Materials 2nd ed, (John Wiley & Sons, 2008).
[34] Amrut S. Lanje, Satish J. Sharma, Ramchandra B. Pode, Archives of Physics Research, **1**(1), 49 (2010).
[35] N. M. Deraz, Int. J. Electrochem. Sci., **7**, 4608 (2012).
[36] G. F. Goya, F. C. Fonseca, R. F. Jardim, R. Muccillo, N. L. V. Carreno, E. Longo, E. R. Leite, J. Appl. Phys., **93**(10), Parts 2 & 3, 15 May (2003).
[37] J.-H. Hwang, V. P. Dravid, M. H. Teng, J. J. Host, B. R. Elliott, D. L. Johnson, T. O. Mason, J. Mater. Res., **12**(4), Apr (1997).
[38] Carey R., Isaac E.D., Magnetic domains and techniques for their observation, (The English University Press Ltd, London, 1966).
[39] D. J. Dunlop, B. Carter-Stiglitz, J. Geophys. Res. 111, B12S09, doi:10.1029/ 2006JB004499 (2006).
[40] J. M. D. Coey, Magnetism and Magnetic Materials, (Cambridge Univ. Press, 2010).
[41] Kuan-Yu Lin, Wen-Ta Tsai, Jeng-Kuei Chang, International Journal of Hydrogen Energy **35**, 7555(2010).
[42] C. Burda, X. Chen, R. Narayanan, M. A. El-Sayed., Chem Rev. **105**, 1025 (2005).
[43] R. W. Murray, Chem Rev. 10**8**, 2688 (2008).
[44] Tao Fei Fei, Xu Zheng, Acta Phys. Chim. Sin., **25**(5), 977 (2009).

*Corresponding author: elaela11@yahoo.com